ATPIF1 alleviates oxygen glucose deprivation/reoxygenation-induced astrocyte injury in vitro: A rat model of ischemic brain injury

Zhijie Wei[1,2,A–D,F], Rui Wu[2,A–C,F], Li Zhang[2,A–C,F], Ping Xu[2,A,C,E,F]

[1] Department of Neurology, Soochow University, China
[2] Department of Neurology, Affiliated Hospital of Zunyi Medical University, China

A – research concept and design; B – collection and/or assembly of data; C – data analysis and interpretation;
D – writing the article; E – critical revision of the article; F – final approval of the article

Advances in Clinical and Experimental Medicine, ISSN 1899–5276 (print), ISSN 2451–2680 (online) *Adv Clin Exp Med*. 2023;32(7):791–802

Address for correspondence
Ping Xu
E-mail: xuping5272021@126.com

Funding sources
The study was supported by Science and Technology Foundation of Guizhou Provincial Health Commission (grant No. Gzwkj2021-025).

Conflict of interest
None declared

Acknowledgements
The authors would like to acknowledge the funder for the financial support.

Received on March 22, 2022
Reviewed on September 1, 2022
Accepted on December 14, 2022

Published online on March 7, 2023

Abstract

Background. The role of ATPIF1 in ischemic brain injury is rarely reported.

Objectives. This study explored the effect of ATPIF1 on astrocyte activity under oxygen glucose deprivation/reoxygenation (OGD/R).

Materials and methods. The study sample was randomly allocated into: 1) control group (blank control); 2) OGD/R group (hypoxia for 6 h/reoxygenation for 1 h); 3) siRNA negative control (NC) group (OGD/R model+siRNA NC); and 4) siRNA-ATPIF1 group (OGD/R model+siRNA-ATPIF1). The OGD/R cell model was established from Sprague Dawley (SD) rats to simulate ischemia/reperfusion injury. Cells in the siRNA-ATPIF1 group were treated with siATPIF1. Ultrastructural changes in the mitochondria were observed using transmission electron microscopy (TEM). Apoptosis, cell cycle, reactive oxygen species (ROS), and mitochondrial membrane potential (MMP) were detected with flow cytometry. The protein expression levels of nuclear factor kappa B (NF-κB), B-cell lymphoma 2 (Bcl-2), Bcl-2-associated X (Bax), and caspase-3 were detected with western blot.

Results. In the model group, the cell structure and the ridge structure were destroyed, and mitochondria edema, outer membrane damage and vacuole-like lesions were observed. Compared with the control group, the OGD/R group had considerably increased apoptosis, G0/G1 phase, ROS content, MMP, and Bax, caspase-3 and NF-κB protein expression, as well as markedly decreased S phase and Bcl-2 protein expression. Compared with the OGD/R group, the siRNA-ATPIF1 group had considerably decreased apoptosis, G0/G1 phase, ROS content, MMP, and Bax, caspase-3 and NF-κB protein expression, as well as remarkably increased S phase and Bcl-2 protein expression.

Conclusions. The inhibition of ATPIF1 may alleviate OGD/R-induced astrocyte injury by regulating the NF-κB signaling pathway, inhibiting apoptosis, and reducing the ROS content and MMP in the rat brain ischemic model.

Key words: apoptosis, NF-κB signaling pathway, OGD/R, astrocytes, ATPIF1

Cite as
Wei Z, Wu R, Zhang L, Xu P. ATPIF1 alleviates oxygen glucose deprivation/reoxygenation-induced astrocyte injury in vitro: A rat model of ischemic brain injury. *Adv Clin Exp Med*. 2023;32(7):791–802. doi:10.17219/acem/157477

DOI
10.17219/acem/157477

Background

Ischemic cerebrovascular disease has been the leading cause of disability and mortality globally.[1,2] A variety of biochemical mechanisms are involved in the pathophysiological process of the disease, including brain energy metabolism disorder, reactive oxygen species (ROS) production, inflammation, acidosis, and apoptosis.[3] As the most widely distributed and numerous cells in the brain, astrocytes are very important for maintaining neuronal structure and function.[4,5] When ischemic injury occurs, astrocytes can fill the damaged area, maintain the stability of the environment in the central nervous system, provide nutrients for neurons, and protect neurons; thus, they are crucial for the repair of an ischemic area and to avoid the secondary injury of neurons.[6]

All cell activities are inseparable from adenosine triphosphate (ATP) consumption; hence, ATP synthesis and decomposition in astrocytes are of great importance after the ischemic injury. Mitochondrial ATPase inhibitor, ATPIF1, is a nuclear coding protein that can interact with ATP synthase.[7] The ATPIF1 is the most characteristic regulator of F1Fo-ATP synthase. It combines with enzymes inhibiting its hydrolytic activity to protect cells from ATP consumption.[8] The ATPIF1 has been associated with a variety of diseases, such as diabetic nephropathy, breast cancer and anemia.[9–12] The ATPIF1 can aggravate the development of diabetic nephropathy by inducing mitochondrial damage.[9] The inhibition of ATPIF1 can improve the severe decrease in electron transport chain activity in mitochondrial pathology.[10] However, the role of ATPIF1 in ischemic brain injury is rarely reported.

In biological systems, the mitochondria are the main place for cells to generate energy. They are also the key intracellular targets for initiating the intrinsic pathway of apoptosis.[13] The ATPIF1 abnormality causes a series of chain reactions in the mitochondria. The mitochondria are the main part of ROS production in tissues. Increased ROS levels can induce apoptosis through endogenous and exogenous pathways.[14] Nuclear factor kappa B (NF-κB) is a traditional transcription factor. It regulates the apoptosis program through its downstream target genes under different stimuli, such as ROS accumulation and inflammatory factors.[15] However, the role of ATPIF1 in astrocyte apoptosis mediated by oxygen glucose deprivation/reoxygenation (OGD/R) remains unknown.

Objectives

The aim of this study was to explore the effect of ATPIF1 on astrocyte activity in Sprague Dawley (SD) rats under OGD/R. We hypothesized that siATPIF1 has a protective effect on the astrocyte activity in OGD/R-induced astrocyte injury. The findings of this study may help develop a feasible approach to treating ischemic cerebrovascular disease.

Materials and methods

Ethics declarations

The Animal Care and Use Committee of the Affiliated Hospital of Zunyi Medical University, China, has given the approval to the experiments and protocol used in this study (approval No. 2020041501).

Experimental animals

Specific pathogen-free SD rats (female, 3 months old; male, 9 months old; license No. SCXK (Xiang) 2019-0014) were obtained from Changsha Tianqin Biotechnology Co., Ltd. (Hunan, China) and raised under 30–70% humidity, 20–26°C and 12 h/12 h light/dark cycle. The rats were allowed food and water ad libitum.

Primary cell isolation and identification

The rats were caged together with a male–female ratio of 1:2, and the neonatal rats were used for further experiments. No gender requirement was set for the neonatal rats. A total of 4 litters with about 12 neonatal rats in each litter were used. The neonatal rats were given sodium pentobarbital (45 mg/kg; MilliporeSigma, Burlington, USA). The brains of the rats were removed following cervical dislocation after immersion and disinfection with 75% ethanol for 1 min. The pia mater covered on the surface of the brain tissue was stripped, and the rat cerebral cortex was separated and washed repeatedly with D-Hank's solution (Beijing Solarbio Science & Technology Co., Ltd., Beijing, China). The washed cortex was repeatedly ground and sieved (220 mesh screen). The screen was repeatedly washed and the cell suspension was transferred to a 15-milliliter clean tube. The pooled samples were centrifuged at 4°C (1500 rpm) for 5 min. The supernatant was discarded, the precipitate was resuspended in Dulbecco's modified Eagle's medium (DMEM; Gibco, Thermo Fisher Scientific, Waltham, USA) containing 10% fetal bovine serum (FBS; Beijing Solarbio Science & Technology Co., Ltd.), and the cells were cultured in 5% CO_2 at 37°C. The medium was replaced with a fresh medium every 3 days. When the cells reached 90% confluence, they were placed in a 37°C shaker incubator for 4–6 h. Then, the microglia supernatant was removed.

The cell climbing sheets were washed with 0.1 M phosphate-buffered saline (PBS), fixed with 4% paraformaldehyde (Beijing Solarbio Science & Technology Co., Ltd.) at room temperature (RT) for 15 min, and blocked for 40 min with 3% goat serum (Beijing Solarbio Science & Technology Co., Ltd.) and 0.1% Triton X-100 (MilliporeSigma). The cells were incubated with rabbit anti-glial fibrillary acidic protein (anti-GFAP) primary antibody (1:200, AB53554; Abcam, Cambridge, UK) at 4°C overnight and IgG/Cy3 fluorescent secondary antibody (1:200,

A0502; Beyotime Biotechnology Inc., Shanghai, China) at RT for 60 min. Then, 4',6-diamidino-2-phenylindole (DAPI; Jiangsu KeyGen Biotech Corp., Ltd., Jiangsu, China) was applied and incubated for 3 min. The cells were mounted with 95% glycerol and observed using a fluorescence microscope (model CX41; Olympus Corp., Tokyo, Japan).

OGD/R cell model

Third-generation astrocytes with good growth condition were selected and 0.125% trypsin (Beijing Solarbio Science & Technology Co., Ltd.) was added for digestion. The cells were centrifuged at 1500 rpm for 5 min and the precipitation was resuspended. The cells were seeded in a 6-well culture plate (1×10^5/well) and cultured in sugar-free DMEM with 94% N_2, 5% CO_2 and 1% O_2 at 37°C for 24 h. The cells were collected and detected at 1, 3, 6, and 24 h.

Cell transfection

The cells were cultured in a 6-well plate. Cell transfection was performed when they reached 70% confluence. Lipofectamine 3000 kit (Invitrogen, Thermo Fisher Scientific, Waltham, USA) was used. A 12.5 µL small interfering RNA (siRNA) was mixed with 125 µL of Opti-MEM (Gibco) and 5 µL of Lipofectamine 3000 was mixed with 125 µL of Opti-MEM. Both mixtures were separately incubated at RT for 5 min, then mixed, incubated for 15 min at RT, and added to the cells cultured in the 6-well plate for 4 h. The cells were cultured in DMEM/F-12 complete medium (Gibco) containing 20% FBS (BBI Life Sciences Corp., Shanghai, China).

The transcription sequences were obtained from the National Center for Biotechnology Information (NCBI; https://www.ncbi.nlm.nih.gov/). The target gene sequences were handed over to General Biol Co., Ltd. (Anhui, China), which directly provided the siRNA. The siRNA sequences are shown in Table 1.

Table 1. siRNA sequences

siRNA	siRNA sequence
siATPIF1-1	CGGCAUAAGAAGAAGAUUATT UAAUCUUCUUCUUAUGCCGTT
siATPIF1-2	AGAGAAGGCUGAAGAGGAUTT AUCCUCUUCAGCCUUCUCUTT
siATPIF1-3	GCACCAUGAAGAUGAGAUUTT AAUCUCAUCUUCAUGGUGCTT
NC	UUCUCCGAACGUGUCACGUTT ACGUGACACGUUCGGAGAATT

NC – negative control.

Experimental grouping

The experimental grouping was randomly divided into:

1) control group (blank control);
2) OGD/R group (hypoxia for 6 h/reoxygenation for 1 h);
3) siRNA negative control (NC) group (OGD/R model +siRNA NC);
4) siRNA-ATPIF1 group (OGD/R model+siRNA-ATPIF1).

The investigators performing the subsequent experiments were blinded to the group allocation.

Quantitative real-time polymerase chain reaction

The cells were collected and Trizol reagent (CWBIO, Jiangsu, China) was used for the total RNA extraction. Reverse transcription to cDNA was performed with a HiFiScript cDNA Synthesis Kit (Vazyme Biotech, Jiangsu, China) according to the kit instructions. Quantitative PCR was conducted with a quantitative real-time polymerase chain reaction (qPCR) system (CFX Connect; Bio-Rad, Hercules, USA). The reaction system and reaction steps are presented in Table 2. The primers are shown in Table 3. The β-actin (Sino Biological Inc., Beijing, China) served as the internal control. The relative ATPIF1 mRNA expression was determined based on the $2^{-\Delta\Delta Ct}$ method.

Table 2. Reaction system and reaction steps of quantitative real-time polymerase chain reaction (qPCR) system

Reagent	Volume	
RNase free dH_2O	9.5 µL	
cDNA	1 µL	
Forward primer	1 µL	
Reverse primer	1 µL	
2× SYBR Green PCR Master Mix	12.5 µL	
Step	**Temperature**	**Time**
Pre-denaturation	95°C	10 min
Denaturation	95°C	10 s
Annealing	58°C	30 s
Extension	72°C	30 s
Number of cycles	40	

Table 3. Primers of quantitative real-time polymerase chain reaction (qPCR)

Primer	Sequence	Length [nt]	Product length [bp]	Annealing temperature [°C]
ATPIF1 F	CTCGGTGTCTGGGGTATGA	19	252	56.81
ATPIF1 R	ATGCCGTTCGATCTGTTTT	19		
β-actin F	GCCATGTACGTAGCCATCCA	20	375	59.5
β-actin R	GAACCGCTCATTGCCGATAG	20		

Western blot

The cells were lysed in the radioimmunoprecipitation (RIPA) buffer (Applygen Technologies Inc., Beijing, China) at 4°C for 30 min and then centrifuged at 12,000 rpm for 10 min. For total protein determination, the supernatant was carefully extracted, and determination was conducted according to the Bradford method (Beijing Solarbio Science & Technology Co., Ltd.). This step was followed by protein denaturation and sample loading. Sodium dodecyl sulfate-polyacrylamide gel electrophoresis (SDS-PAGE; Xilong Scientific Co., Ltd., Guangdong, China) was performed for 2 h before transferring to polyvinylidene fluoride membrane (PVDF; MilliporeSigma) at 300 mA. The primary antibodies used included mouse monoclonal anti-glyceraldehyde 3-phosphate dehydrogenase (anti- GAPDH; 1:2000, cat. No. TA-08; ZSGB-BIO, Beijing, China), mouse anti-ATPIF1 (1:1000, ab110277; Abcam), mouse anti-B-cell lymphoma 2 (anti-Bcl-2; 1:1000, cat. No. 60178-1-Ig; Proteintech, Rosemont, USA), rabbit anti-Bcl-2-associated X (anti-Bax; 1:1000, cat. No. 50599-2-Ig; Proteintech), rabbit anti-nuclear factor-kappa B (anti-NF-κB; 1:1000, 10745-1-AP; Proteintech), and rabbit anti-caspase-3 (1:1000, cat. No. YT0656; ImmunoWay Biotechnology Co., Plano, USA). The primary antibodies were added and incubated at 4°C overnight. Then, the secondary antibodies were added and incubated at RT for 2 h. The secondary antibodies used included goat anti-rabbit IgG antibody (H+L, horseradish peroxidase (HRP)-conjugated, 1:2000, cat. No. ZB-2301) and goat anti-mouse IgG antibody (H+L, HRP-conjugated, 1:2000, cat. No. ZB-2305; ZSGB-BIO). The chemiluminescent substrate was added, and the membrane was examined using a gel imaging system (ChemiDoc XRS+; Bio-Rad). The blot was analyzed using Quantity One software v. 4.62 (Bio-Rad) with GAPDH as the internal reference, using the equation: relative protein expression = (target protein integral optical density (IOD) / internal reference protein IOD).

Detection with flow cytometry

Apoptosis

The cells (1×10^6–3×10^6) were collected. An Annexin V–Propidium Iodide (PI) Analysis Kit (MultiSciences (Lianke) Biotech Co., Ltd., Hangzhou, China) was used for apoptosis detection based on the manufacturer's instructions. The cells were washed 3 times with precooled PBS, resuspended with 300 µL of ×1 binding buffer, added with 3 µL of Annexin V-fluorescein isothiocyanate (FITC) and 5 µL of PI-phycoerythrin solution, and mixed gently. Then, the cells were incubated in the dark at RT (20–25°C) for 10–20 min and placed in an ice bath. The detection was performed on a NovoCyte™ flow cytometer (NovoCyte 2060R; ACEA Bio (Hangzhou) Co., Ltd., Hangzhou, China).

Cell cycle

The cells were collected, washed with PBS, 1 mL of DNA staining solution and 10 µL of PI solution were added, and the cells were mixed. Then, they were incubated in the dark at RT for 30 min. The cell cycle was determined with flow cytometry.

ROS

The cells were harvested and a final concentration of 10 µM 2',7'-dichlorofluorescein diacetate (DCFH-DA) solution (Reactive Oxygen Species Assay Kit; Jiangsu KeyGEN BioTECH Co., Ltd.) was obtained with1:1000 dilution of DCFH-DA in serum-free medium. The cell culture medium was replaced with the diluted DCFH-DA. The cells were incubated at 37°C for 20 min and then washed 3 times with serum-free medium and 3 times with PBS. The ROS levels were determined with flow cytometry.

Membrane potential

The cells were collected, washed with PBS and centrifuged at 2000 rpm for 5 min. Next, the cells were resuspended with 500 µL of JC-1 solution (BestBio, Shanghai, China) and cultured at 37°C with 5% CO_2 for 15–20 min. Then, they were centrifuged at 2000 rpm for 5 min, washed twice with ×1 incubation buffer, resuspended with 500 µL of ×1 incubation buffer, and analyzed with flow cytometry.

Statistical analyses

Data analysis was performed with GraphPad Prism 7 software (GraphPad Software, San Diego, USA). The comparisons between groups were performed using one-way analysis of variance (ANOVA) with Bonferroni post hoc test. The value of $p < 0.05$ was considered statistically significant.

Outcome measures

The outcome measures were the effects of siATPIF1 on the mitochondrial structure, apoptosis, cell cycle, ROS production, mitochondrial membrane potential (MMP), apoptosis-related genes, and the NF-κB pathway in the OGD/R model.

Results

Isolation and identification of astrocytes

The isolated and purified cells were star-shaped, and many long and branched processes were separated from the cell body. The GFAP is a marker for astrocytes. Immunofluorescence results showed that the nuclei of astrocytes were stained blue and the cells were stained red (GFAP). The purity of astrocytes was more than 95% (Fig. 1).

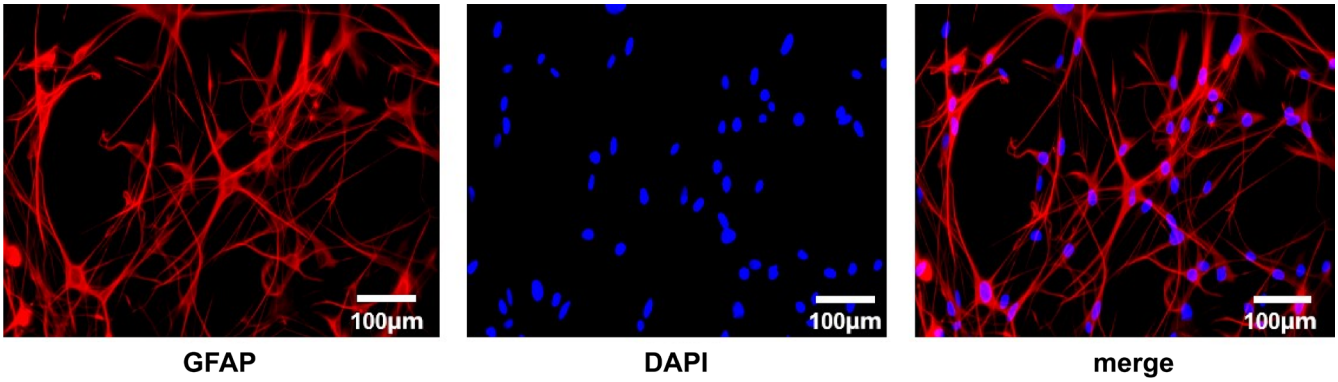

Fig. 1. Astrocyte identification

DAPI – 4′,6-diamidino-2-phenylindole; GFAP – glial fibrillary acidic protein.

Selection of OGD/R model conditions

As shown in Fig. 2A, the apoptosis rate was the highest at 1 h of reperfusion compared with the control group. Many cells were irregular and had mitochondrial edema, outer membrane damage, vacuole-like lesions, or damaged ridge structure at 1 h of reperfusion (Fig. 2B). Moreover, the mitochondria were irregular, some mitochondria were swollen, and the cristae disappeared at 3 h after reperfusion. Finally, the mitochondrial ridge structure was destroyed and became a vacuole-like lesion at 24 h after reperfusion. Figure 2C shows that ATPIF1 protein expression increased remarkably at 1 h of reperfusion. Therefore, the model was established at 1 h of reperfusion in subsequent experiments.

ATPIF1 siRNA transfection efficiency verification

As shown in Fig. 3, the ATPIF1 mRNA expression levels in the siRNA groups (particularly the siATPIF1-2 group) were considerably lower than those in the control and siRNA NC groups. The ATPIF1 protein expression levels in the siRNA-2 and siRNA-3 groups were remarkably lower than in the control and siRNA NC groups. Therefore, siRNA-2 was selected for subsequent experiments.

Effect of siATPIF1 on mitochondrial structure in the OGD/R model

The mitochondrial morphological changes were examined using transmission electron microscopy (TEM). As shown in Fig. 4, the cell morphology in the control group was normal and the ridge structure was complete; the cell and ridge structures in the OGD/R group were destroyed, and mitochondria edema, outer membrane damage or vacuole-like lesions were noted; the cells in the siRNA NC group were irregular, some mitochondria were swollen and cristae disappeared; the cell and mitochondrial membrane structures in the siRNA-ATPIF1 group were complete, and most of the ridge structures were normal.

Effects of siATPIF1 on apoptosis and cell cycle in the OGD/R model

The apoptosis rate in the OGD/R group was considerably higher than in the control group, whereas the apoptosis rate in the siRNA-ATPIF1 group was substantially lower than in the OGD/R group (Fig. 5A). The OGD/R group had a remarkably increased G0/G1 and a remarkably decreased S phase compared with the control group. Moreover, the siRNA-ATPIF1 group had a considerably decreased G0/G1 phase and substantially increased S phase compared with the OGD/R group (Fig. 5B).

Effects of siATPIF1 on ROS and MMP in the OGD/R model

The ROS levels in the OGD/R group were significantly increased compared with the control group; the ROS levels in the siRNA-ATPIF1 group were significantly decreased compared with the OGD/R group (Fig. 6A). The MMP in the OGD/R group was considerably increased compared with the control group, and the MMP in the siRNA-ATPIF1 group was remarkably decreased compared with the OGD/R group (Fig. 6B).

Effects of siATPIF1 on apoptosis-related genes and NF-κB pathway in the OGD/R model

The western blot results are shown in Fig. 7. The OGD/R group had substantially increased Bax, caspase-3 and NF-κB protein expression, and remarkably decreased Bcl-2 protein expression compared with the control group. The siRNA-ATPIF1 group had remarkably decreased Bax, caspase-3 and NF-κB protein expression levels, and increased Bcl-2 protein expression compared with the OGD/R group.

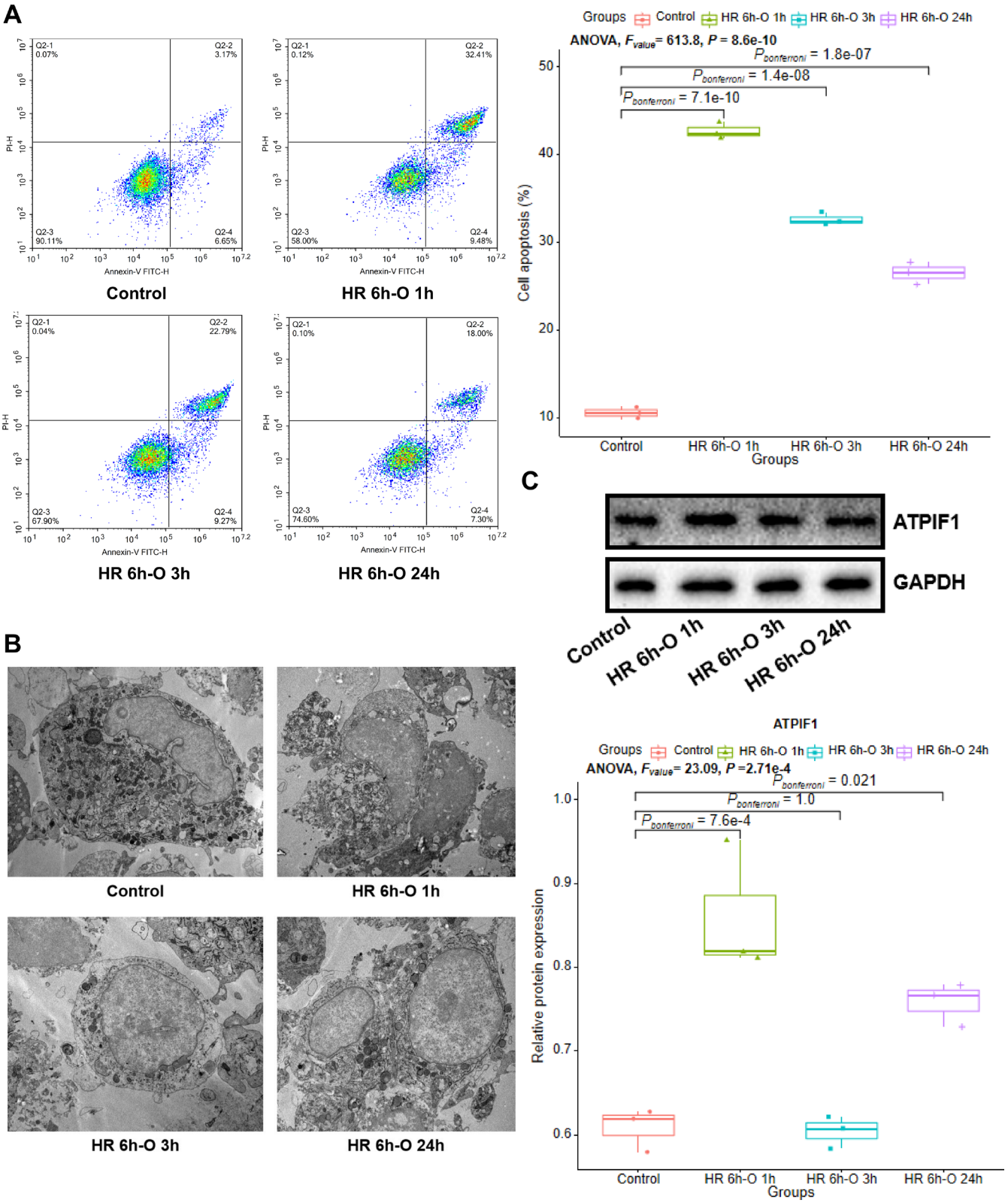

Fig. 2. Selection of oxygen glucose deprivation/reoxygenation (OGD/R) model. A. Scatter plots of cell apoptosis (analysis of variance (ANOVA), F = 613.8, p = 8.6e-10; Hypoxia reoxygenation (HR) 6h-O 1h compared to controls, $p_{bonferroni}$ = 7.1E-10; HR 6h-O 3h compared to controls, $p_{bonferroni}$ = 1.4E-08; HR 6h-O 24h compared to controls, $p_{bonferroni}$ = 1.8E-07); B. Ultrastructural changes in the mitochondria determined using transmission electron microscopy (TEM); C. ATPIF1 protein expression (ANOVA, F = 23.09, p = 0.000271; HR 6h-O 1h compared to controls, $p_{bonferroni}$ = 7.6E-04; HR 6h-O 3h compared to controls, $P_{bonferroni}$ = 1.0000; HR 6h-O 24h compared to controls, $p_{bonferroni}$ = 0.0213). The data analysis results are presented in Supplementary Table 1

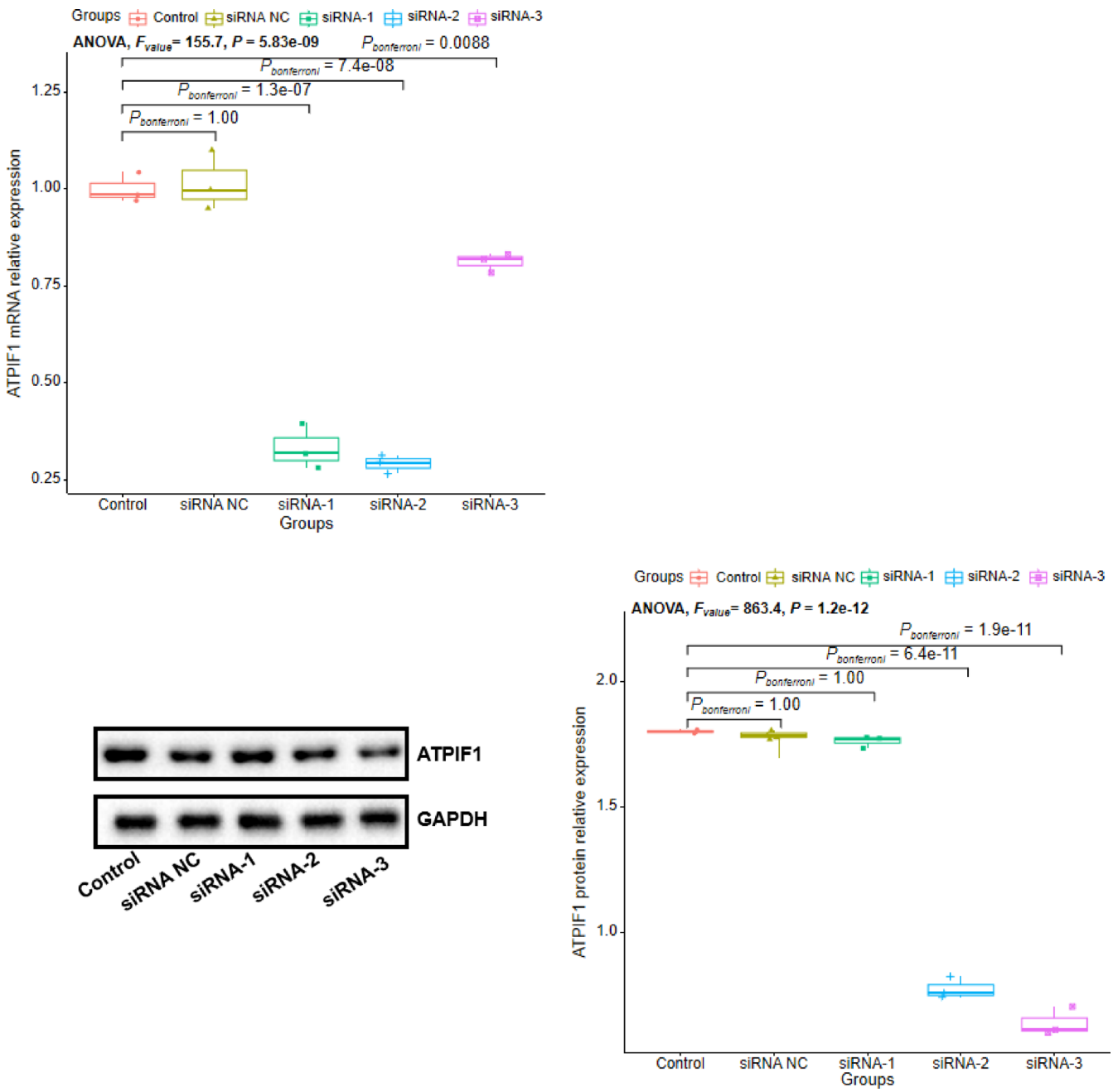

Fig. 3. The ATPIF1 siRNA transfection efficiency in each group. ATPIF1 mRNA relative expression: analysis of variance (ANOVA), F = 155.7, p = 5.83e-09; siRNA-1 compared to controls, $p_{bonferroni}$ = 1.3E-07, compared to siRNA NC, $p_{bonferroni}$ = 1.0E-07; siRNA-2 compared to controls, $P_{bonferroni}$ = 7.4E-08, compared to siRNA NC, $p_{bonferroni}$ = 6.0E-08; siRNA-3 compared to controls, $p_{bonferroni}$ = 0.0088, compared to siRNA NC, $p_{bonferroni}$ = 0.005. The ATPIF1 protein relative expression: ANOVA, F = 863.4, p = 1.2e-12; siRNA-1 compared to controls, $p_{bonferroni}$ = 1.0000, compared to siRNA NC, $p_{bonferroni}$ = 1.0000; siRNA-2 compared to controls, $p_{bonferroni}$ = 6.4E-11, compared to siRNA NC, $p_{bonferroni}$ = 7.4E-11; siRNA-3 compared to controls, $p_{bonferroni}$ = 1.9E-11, compared to siRNA NC, $p_{bonferroni}$ = 2.1E-11. The data analysis results are presented in Supplementary Table 1

Discussion

Evidence of the relationship between ischemic brain injury and increased astrocyte injury has been found in previous research.[16] Astrocytes are the most abundant cell type in the central nervous system.[17] They communicate with neurons, oligodendrocytes and endothelial cells, and participate in maintaining normal brain function.[18] Therefore, astrocytes have become the neuroprotective target in ischemic brain injury.[19] The ATPIF1 is a mitochondrion-localized protein encoded by nuclear DNA. The ATPIF1 can inhibit ATP hydrolysis through ATP synthase when bound to F1 complexes α and β.[20] The ATPIF1 regulates mitochondrial morphology and cell survival.[21] Our study demonstrated that siRNA-ATPIF1 may protect astrocytes from OGD/R-induced apoptosis and necrosis by maintaining mitochondrial anti-apoptosis (Bcl-2 upregulation) and bioenergetic function.

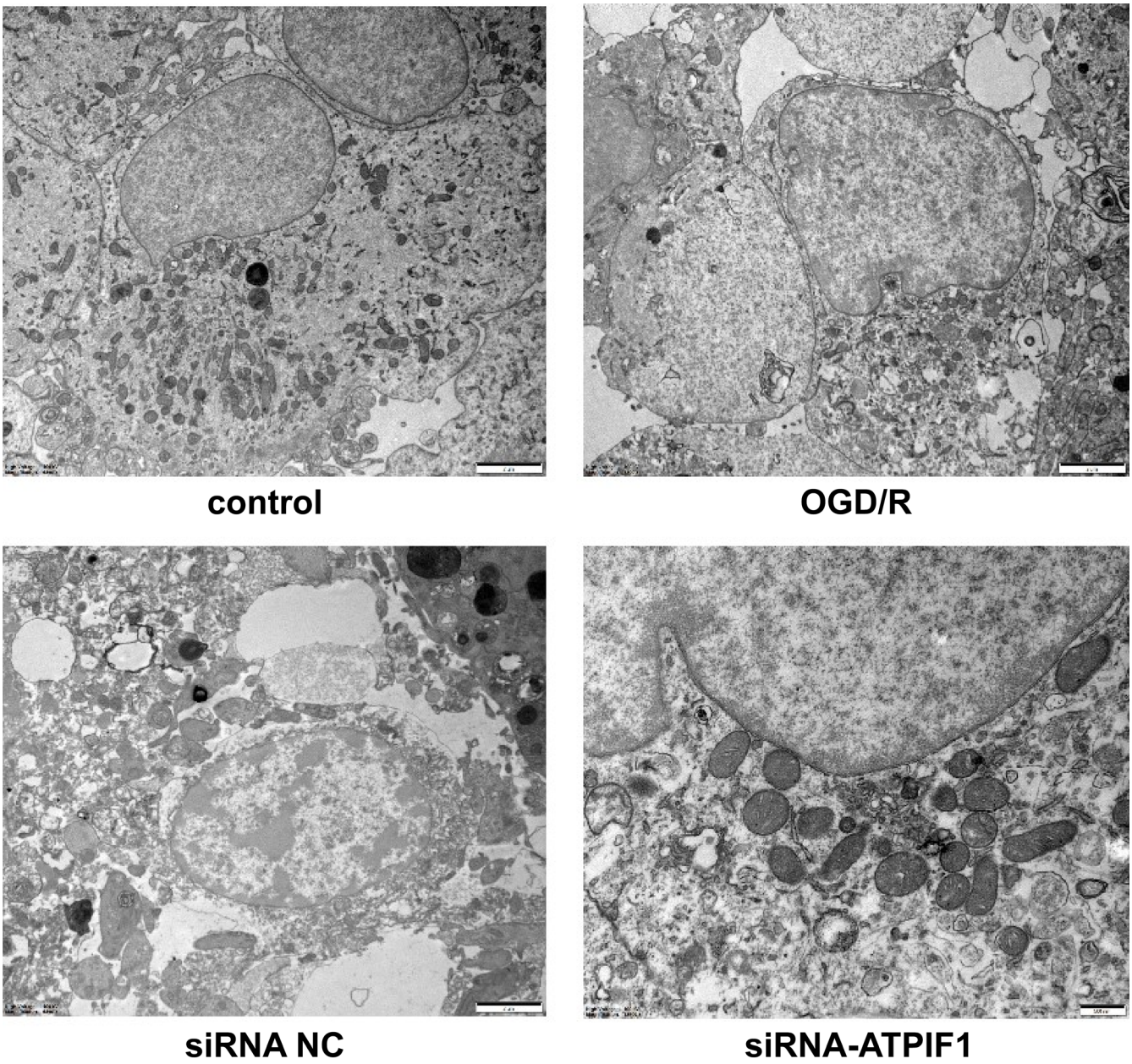

Fig. 4. Morphological changes in the mitochondria in each group

OGD/R – oxygen glucose deprivation/reoxygenation.

Apoptosis can be induced by extrinsic (death receptor) and intrinsic (mitochondrial) pathways.[22] Mitochondrial morphology changes in the mitochondria-mediated pathway. The increase in mitochondrial membrane permeability causes the activation of downstream effector caspases, such as caspase-3, and eventually induces apoptosis.[23] Xu et al. demonstrated that ATPIF1 plays a key role in regulating cleaved caspase-3 expression in the microglia.[24] The Bcl-2 family proteins, such as Bax and Bcl-2, mediate the intrinsic pathway by altering the outer membrane permeability of the mitochondria.[25] The Bax protein is a common channel of the mitochondria-mediated apoptosis pathway.[26] We found that siRNA-ATPIF1 could inhibit Bax and increase Bcl-2 protein expression in astrocytes. The OGD/R-induced astrocytes had increased MMP and abnormal mitochondrial morphology, and siRNA-ATPIF1 inhibited these processes. Cleaved caspase-3 expression decreased in the OGD/R cells treated with siRNA-ATPIF1. The results showed that siRNA-ATPIF1 could effectively inhibit mitochondria-mediated apoptosis in astrocytes after the OGD/R treatment.

The NF-κB plays an active role in apoptosis.[27] In a non-stimulated state, NF-κB and IκB form a complex in the cytoplasm, but they are not activated. The IκB is rapidly phosphorylated after cell stimulation and further degraded

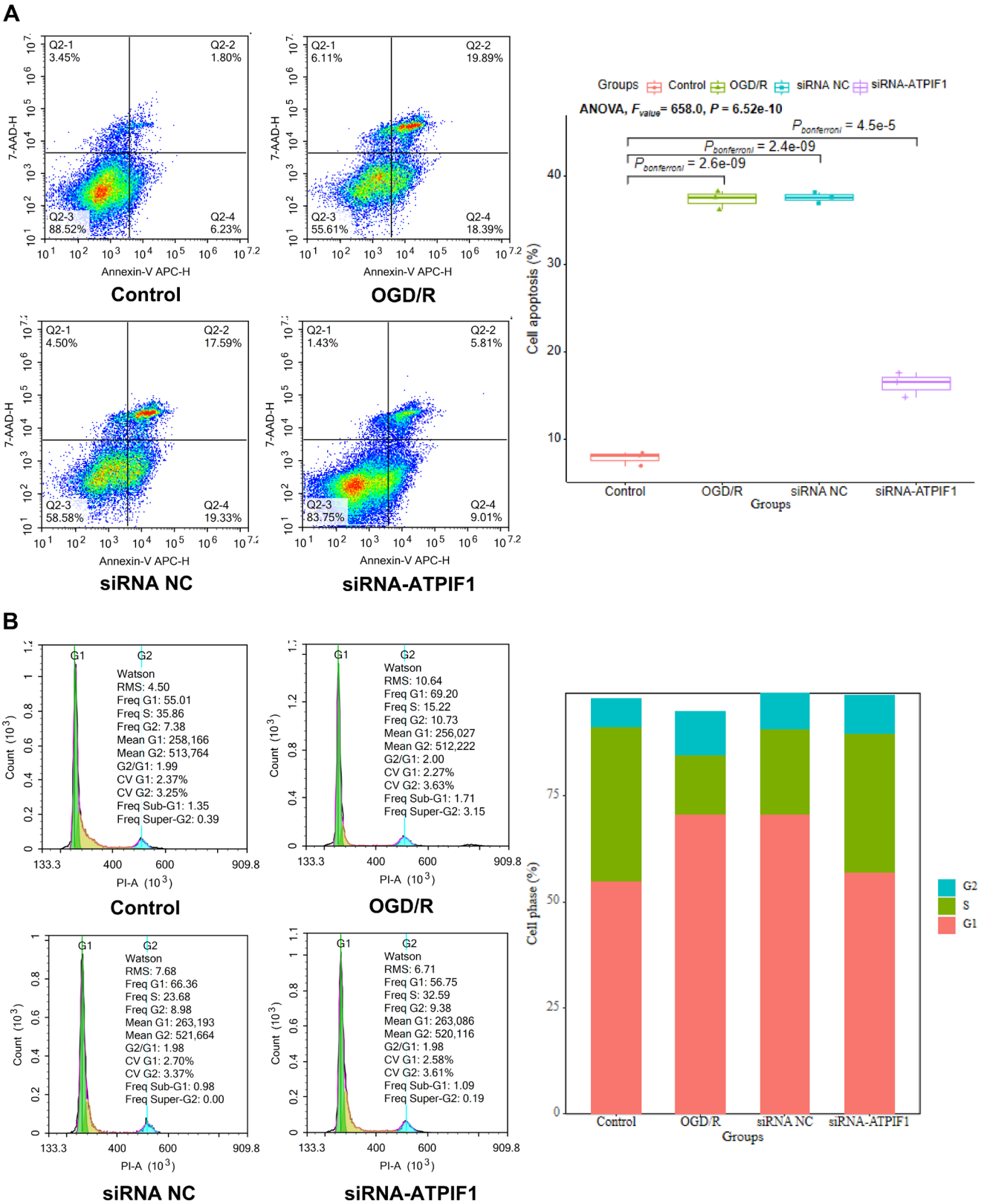

Fig. 5. Apoptosis and cell cycle detected using flow cytometry. A. Scatter plots of cell apoptosis (analysis of variance (ANOVA), F = 658.0, p = 6.52e-10; oxygen glucose deprivation/reoxygenation (OGD/R) compared to controls, $p_{bonferroni}$ = 2.6E-09; siRNA-ATPIF1 compared to OGD/R, $p_{bonferroni}$ = 0.000000037); B. Cell cycle. The data analysis results are presented in Supplementary Table 1

by ubiquitinase or protease.[28] After IκB degradation is complete, NF-κB is rapidly activated and then translocated into the nucleus to react with the downstream targets.[29] The NF-κB can respond to ROS accumulation signals and initiate the pro-apoptotic pathway activation.[30] The present study found that astrocytes produce

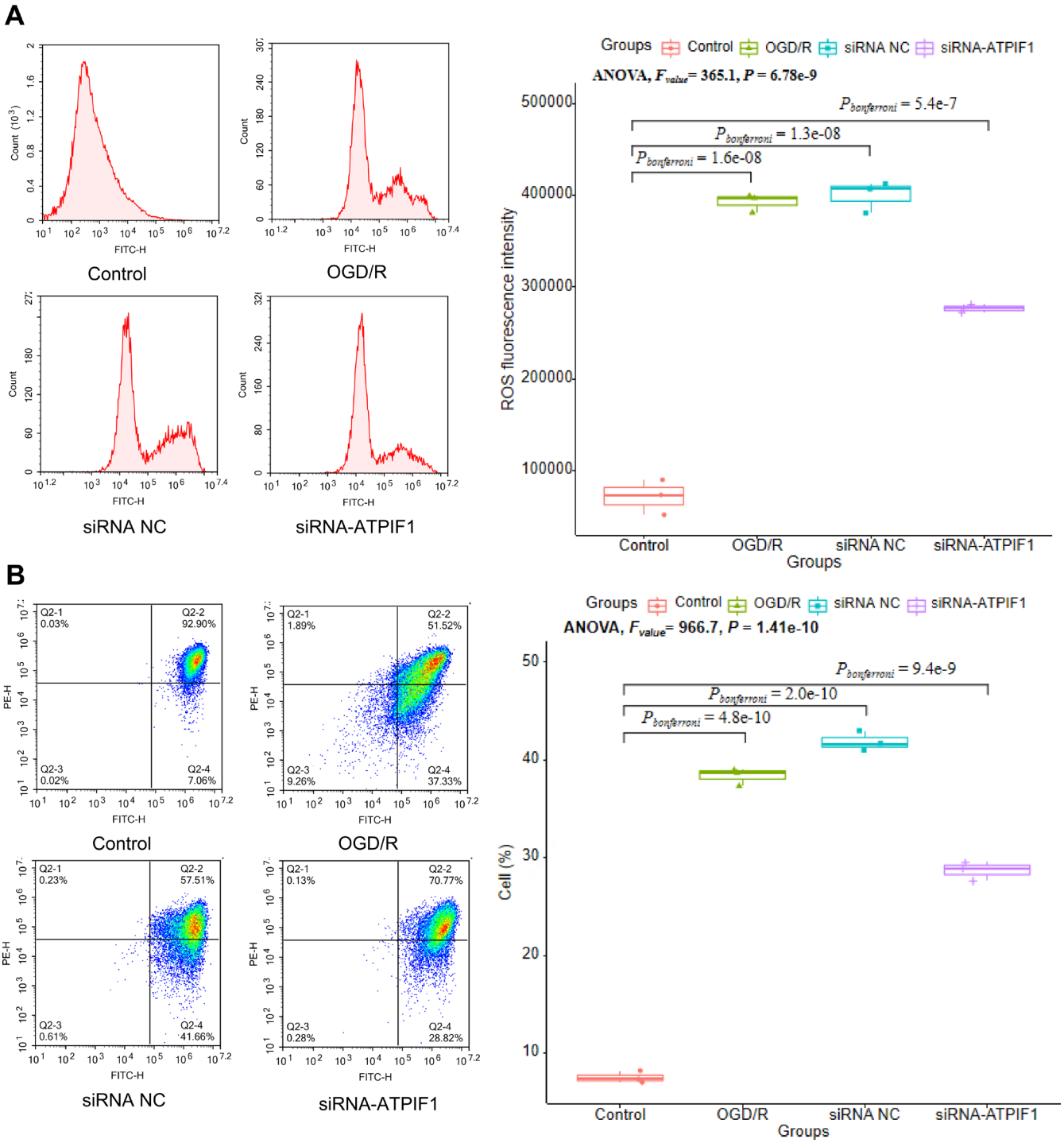

Fig. 6. Reactive oxygen species (ROS) and membrane potential detected using flow cytometry. A. ROS level (analysis of variance (ANOVA), F = 365.1, p = 6.78e-09; oxygen glucose deprivation/reoxygenation (OGD/R) compared to controls, p = 0.000000016; siRNA-ATPIF1 compared to OGD/R, $p_{bonferroni}$ = 4.3E-05); B. Membrane potential (ANOVA, F = 966.7, p = 1.41e-10; OGD/R compared to controls, $p_{bonferroni}$ = 4.8E-10; siRNA-ATPIF1 compared to OGD/R, $p_{bonferroni}$ = 4.6E-06). The data analysis results are presented in Supplementary Table 1

a large amount of ROS after OGD/R. Therefore, we investigated whether NF-κB is involved in ATPIF1-mediated mitochondrial apoptosis. Western blot results showed that ATPIF1 knockdown could reduce NF-κB expression, indicating that the NF-κB signaling pathway may be involved in ATPIF1-induced mitochondrial apoptosis in astrocytes.

Limitations

Although this study has clarified the effect of ATPIF1 on astrocyte apoptosis, some studies have pointed out that pH changes also have a remarkable effect on ATPIF activity.[31] However, this factor was not taken into account in our experiments. The effect of hypoxia on pH value in vivo and

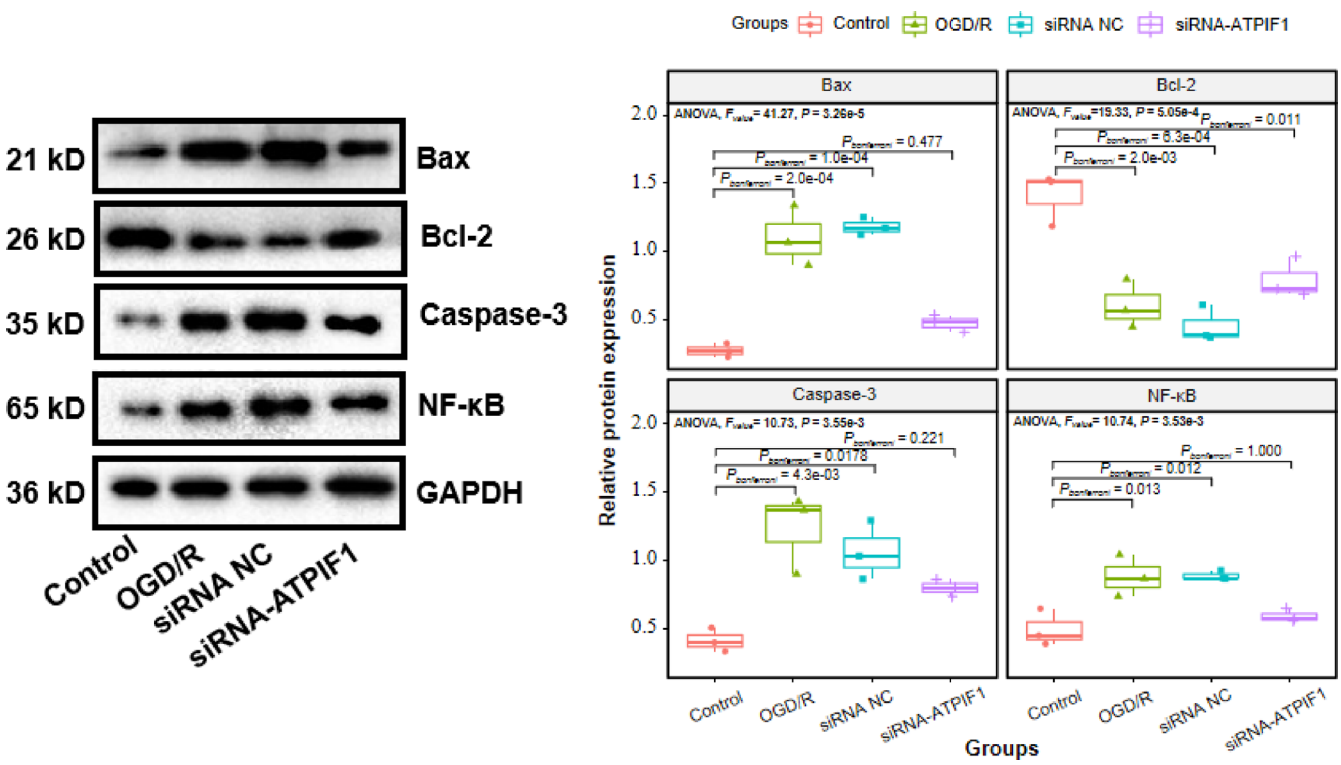

Fig. 7. Bcl-2-associated X (Bax), B-cell lymphoma 2 (Bcl-2), caspase-3, and nuclear factor kappa B (NF-κB) protein expression. Bax: analysis of variance (ANOVA), F = 41.27, p = 3.26e-05; oxygen glucose deprivation/reoxygenation (OGD/R) compared to controls, $p_{bonferroni}$ = 2.0E-04; siRNA-ATPIF1 compared to OGD/R, $p_{bonferroni}$ = 0.001. Bcl-2: ANOVA, F = 19.33, p = 0.000505; OGD/R compared to controls, $p_{bonferroni}$ = 2.0E-03; siRNA-ATPIF1 compared to controls, $p_{bonferroni}$ = 0.011, compared to OGD/R, $p_{bonferroni}$ = 1.000. Caspase-3: ANOVA, F = 10.73, p = 0.00355; OGD/R compared to controls, $p_{bonferroni}$ = 0.0043; siRNA-ATPIF1 compared to controls, $p_{bonferroni}$ = 0.221, compared to OGD/R, $p_{bonferroni}$ = 0.135. NF-κB: ANOVA, F = 10.74, p = 0.00353; OGD/R compared to controls, $p_{bonferroni}$ = 0.013, siRNA-ATPIF1 compared to controls, $p_{bonferroni}$ = 1.000, compared to OGD/R, $p_{bonferroni}$ = 0.061. The data analysis results are presented in Supplementary Table 1

then on ATPIF1, particularly in animals and even in humans, will also be a direction of our subsequent studies.

Recently, the application of ATPIF1 gene-silenced T cells in the preparation of antitumor drugs has also been described, which provides a new direction for the research and development of adoptive immunotherapy for tumors. We believe that cell therapy by *ATPIF1* gene knockout can have a broad development prospect in the treatment of cerebral ischemia injury.

Conclusions

This study is the first to report that during ischemic brain injury, ATPIF1 regulation of mitochondria-mediated apoptosis is associated with the promotion of NF-κB activation. The ATPIF1 knockdown can improve the mitochondrial morphology, inhibit MMP, massive ROS accumulation and NF-κB activation, reduce Bax expression, increase Bcl-2 protein expression, and maintain astrocyte viability in OGD/R-induced injury.

Generalizability/translation

The findings of this study may be generalized to other species or experimental conditions, including human biology.

Data availability statement

Data will be made available by the corresponding author upon reasonable request.

Supplementary files

The supplementary files are available at https://doi.org/10.5281/zenodo.7454344. The package contains the following files:

Supplementary Table 1. Data analysis for Fig. 2,3,5,6,7.

ORCID iDs

Zhijie Wei https://orcid.org/0000-0001-9593-5084
Rui Wu https://orcid.org/0000-0003-3921-456X
Li Zhang https://orcid.org/0000-0001-7958-4720
Ping Xu https://orcid.org/0000-0002-5166-4080

References

1. Radak D, Katsiki N, Resanovic I, et al. Apoptosis and acute brain ischemia in ischemic stroke. *Curr Vasc Pharmacol*. 2017;15(2):115–122. doi:10.2174/1570161115666161104095522
2. Feigin VL, Krishnamurthi RV, Parmar P, et al. Update on the global burden of ischemic and hemorrhagic stroke in 1990–2013: The GBD 2013 Study. *Neuroepidemiology*. 2015;45(3):161–176. doi:10.1159/000441085
3. Avan A, Hachinski V. Stroke and dementia, leading causes of neurological disability and death, potential for prevention. *Alzheimers Dementia*. 2021;17(6):1072–1076. doi:10.1002/alz.12340

4. Wang J, Sareddy GR, Lu Y, et al. Astrocyte-derived estrogen regulates reactive astrogliosis and is neuroprotective following ischemic brain injury. *J Neurosci*. 2020;40(50):9751–9771. doi:10.1523/JNEUROSCI.0888-20.2020
5. Rossi DJ, Brady JD, Mohr C. Astrocyte metabolism and signaling during brain ischemia. *Nat Neurosci*. 2007;10(11):1377–1386. doi:10.1038/nn2004
6. van Putten MJAM, Fahlke C, Kafitz KW, Hofmeijer J, Rose CR. Dysregulation of astrocyte ion homeostasis and its relevance for stroke-induced brain damage. *Int J Mol Sci*. 2021;22(11):5679. doi:10.3390/ijms22115679
7. Kandul NP, Zhang T, Hay BA, Guo M. Selective removal of deletion-bearing mitochondrial DNA in heteroplasmic *Drosophila*. *Nat Commun*. 2016;7(1):13100. doi:10.1038/ncomms13100
8. Martín-Jiménez R, Faccenda D, Allen E, et al. Reduction of the ATPase inhibitory factor 1 (IF_1) leads to visual impairment in vertebrates. *Cell Death Dis*. 2018;9(6):669. doi:10.1038/s41419-018-0578-x
9. Li J, Sun YBY, Chen W, et al. Smad4 promotes diabetic nephropathy by modulating glycolysis and OXPHOS. *EMBO Rep*. 2020;21(2):e48781. doi:10.15252/embr.201948781
10. Chen WW, Birsoy K, Mihaylova MM, et al. Inhibition of ATPIF1 ameliorates severe mitochondrial respiratory chain dysfunction in mammalian cells. *Cell Rep*. 2014;7(1):27–34. doi:10.1016/j.celrep.2014.02.046
11. Kurbasic E, Sjöström M, Krogh M, et al. Changes in glycoprotein expression between primary breast tumour and synchronous lymph node metastases or asynchronous distant metastases. *Clin Proteom*. 2015;12(1):13. doi:10.1186/s12014-015-9084-7
12. Shah DI, Takahashi-Makise N, Cooney JD, et al. Mitochondrial Atpif1 regulates haem synthesis in developing erythroblasts. *Nature*. 2012;491(7425):608–612. doi:10.1038/nature11536
13. Mu W, Cheng X, Zhang X, et al. Hinokiflavone induces apoptosis via activating mitochondrial ROS/JNK/caspase pathway and inhibiting NF-κB activity in hepatocellular carcinoma. *J Cell Mol Med*. 2020;24(14):8151–8165. doi:10.1111/jcmm.15474
14. Wang X, Lu X, Zhu R, et al. Betulinic acid induces apoptosis in differentiated PC12 cells via ROS-mediated mitochondrial pathway. *Neurochem Res*. 2017;42(4):1130–1140. doi:10.1007/s11064-016-2147-y
15. Zhang T, Zhao G, Zhu X, et al. Sodium selenite induces apoptosis via ROS-mediated NF-κB signaling and activation of the Bax–caspase-9–caspase-3 axis in 4T1 cells. *J Cell Physiol*. 2019;234(3):2511–2522. doi:10.1002/jcp.26783
16. Yamagata K. Astrocyte-induced synapse formation and ischemic stroke. *J Neurosci Res*. 2021;99(5):1401–1413. doi:10.1002/jnr.24807
17. Santello M, Toni N, Volterra A. Astrocyte function from information processing to cognition and cognitive impairment. *Nat Neurosci*. 2019;22(2):154–166. doi:10.1038/s41593-018-0325-8
18. Bayraktar OA, Bartels T, Holmqvist S, et al. Astrocyte layers in the mammalian cerebral cortex revealed by a single-cell in situ transcriptomic map. *Nat Neurosci*. 2020;23(4):500–509. doi:10.1038/s41593-020-0602-1
19. Zamboni M, Llorens-Bobadilla E, Magnusson JP, Frisén J. A widespread neurogenic potential of neocortical astrocytes is induced by injury. *Cell Stem Cell*. 2020;27(4):605–617.e5. doi:10.1016/j.stem.2020.07.006
20. Wang K, Chen H, Zhou Z, Zhang H, Zhou HJ, Min W. ATPIF1 maintains normal mitochondrial structure which is impaired by CCM3 deficiency in endothelial cells. *Cell Biosci*. 2021;11(1):11. doi:10.1186/s13578-020-00514-z
21. Faccenda D, Tan CH, Seraphim A, Duchen MR, Campanella M. IF1 limits the apoptotic-signalling cascade by preventing mitochondrial remodelling. *Cell Death Differ*. 2013;20(5):686–697. doi:10.1038/cdd.2012.163
22. Uzdensky AB. Apoptosis regulation in the penumbra after ischemic stroke: Expression of pro- and antiapoptotic proteins. *Apoptosis*. 2019;24(9–10):687–702. doi:10.1007/s10495-019-01556-6
23. Li M, Tan J, Miao Y, Lei P, Zhang Q. The dual role of autophagy under hypoxia-involvement of interaction between autophagy and apoptosis. *Apoptosis*. 2015;20(6):769–777. doi:10.1007/s10495-015-1110-8
24. Xu Y, Gao G, Sun X, Liu Q, Li C. ATPase inhibitory factor 1 is critical for regulating sevoflurane-induced microglial inflammatory responses and caspase-3 activation. *Front Cell Neurosci*. 2021;15:770666. doi:10.3389/fncel.2021.770666
25. Clavier A, Rincheval-Arnold A, Colin J, Mignotte B, Guénal I. Apoptosis in *Drosophila*: Which role for mitochondria? *Apoptosis*. 2016;21(3):239–251. doi:10.1007/s10495-015-1209-y
26. Soond SM, Kozhevnikova MV, Savvateeva LV, Townsend PA, Zamyatnin AA. Intrinsically connected: Therapeutically targeting the cathepsin proteases and the Bcl-2 family of protein substrates as co-regulators of apoptosis. *Int J Mol Sci*. 2021;22(9):4669. doi:10.3390/ijms22094669
27. Khan H, Ullah H, Castilho PCMF, et al. Targeting NF-κB signaling pathway in cancer by dietary polyphenols. *Crit Rev Food Sci Nutr*. 2020;60(16):2790–2800. doi:10.1080/10408398.2019.1661827
28. Soleimani A, Rahmani F, Ferns GA, Ryzhikov M, Avan A, Hassanian SM. Role of the NF-κB signaling pathway in the pathogenesis of colorectal cancer. *Gene*. 2020;726:144132. doi:10.1016/j.gene.2019.144132
29. Kandasamy M. NF-κB signalling as a pharmacological target in COVID-19: Potential roles for IKKβ inhibitors. *Naunyn Schmiedeberg's Arch Pharmacol*. 2021;394(3):561–567. doi:10.1007/s00210-020-02035-5
30. Shen M, Hu Y, Yang Y, et al. Betulinic acid induces ROS-dependent apoptosis and S-phase arrest by inhibiting the NF-κ B pathway in human multiple myeloma. *Oxid Med Cell Longev*. 2019;2019:5083158. doi:10.1155/2019/5083158
31. Cabezón E, Butler PJG, Runswick MJ, Carbajo RJ, Walker JE. Homologous and heterologous inhibitory effects of ATPase inhibitor proteins on F-ATPases. *J Biol Chem*. 2002;277(44):41334–41341. doi:10.1074/jbc.M207169200